Electronic Supplementary Information (ESI)

Cucurbit[6]uril@MIL-101-Cl: loading polar porous cages in mesoporous stable host for enhanced SO_2 adsorption at low pressures

Yangyang Sun,[a] Jun Liang,[a,b] Philipp Brandt,[a] Alex Spieß,[a] Secil Öztürk[a] and Christoph Janiak*[a,b]

[a] Institut für Anorganische Chemie und Strukturchemie, Heinrich-Heine-Universität, 40204 Düsseldorf, Germany.

[b] Hoffmann Institute of Advanced Materials, Shenzhen Polytechnic, 7098 Liuxian Blvd, Nanshan District, Shenzhen 518055, China.

Corresponding author:

E-mail: janiak@uni-duesseldorf.de; Fax: + 49-211-81-12287; Tel: +49-211-81-12286

Additional email addresses:

Yangyang.Sun@uni-duesseldorf.de; liangj956@nenu.edu.cn; p.brandt@hhu.de; alex.spiess@hhu.de; oeztues@uni-duesseldorf.de.

Table of Contents

Table S1 Sources for starting materials and solvents.

Items	Manufacturer
Chromium (III) nitrate nonahydrate	Acros Organics
Benzene-1,4-dicarboxylic acid, H_2BDC	Acros Organics
Urea (> 99.5%)	Sigma–Aldrich
Paraformaldehyde	Carl Roth
Glyoxal (40 wt%)	J&K company
N,N-dimethylformamide	Fisher Chemicals
Nitric acid (65 wt%)	Fisher Chemicals
Hydrochloric acid (37 wt%)	Sigma–Aldrich
Methanol	Sigma–Aldrich
Ethanol	Sigma–Aldrich
Natrium metabisulfite ($Na_2S_2O_5$)	Merck
Sodium chloride	Fischer Scientific

Elemental Analysis:

As a porous material CB6@MIL-101-Cl will adsorb water (humidity) from ambient air during storage and handling in air. Such water content will not give a meaningful CHN analysis as was seen by too high H wt% values.

Therefore, a small amount of sample was activated at 150 °C overnight under vacuum (1×10^{-2} bar), then cooled to room temperature and stored under nitrogen. For CHN analysis the sample was quickly weighed and directly measured.

MIL-101-Cl: $[Cr_3OCl(H_2O)_2(C_8H_4O_4)_3]$ M_w = 735.82 g/mol from which M(C) = is 288.26 g/mol.

CB6: $C_{36}H_{36}N_{24}O_{12}$ M_w = 996.84 g/mol; from which M(N) = is 336.16 g/mol and M(C) = 432.39 g/mol

Found (%) C: 40.35, H: 2.82, N: 10.45

Assuming a formula of the composite as $[Cr_3OCl(H_2O)_2(C_8H_4O_4)_3][C_{36}H_{36}N_{24}O_{12}]_a$

then for the mass fraction of N (w(N) = 0.1045) and C (w(C) = 0.4035), we can establish the two equations:

N: $w(N) = 336.16 \times a : (735.82 + 996.84 \times a)$ (1)

C: $w(C) = (288.26 + 432.39 \times a) : (735.82 + 996.84 \times a)$ (2)

or (1) divided by (2)

$w(N)/w(C) = 336.16 \times a : (288.26 + 432.39 \times a)$

$336.16 \times a = w(N)/w(C) \times (288.26 + 432.39 \times a)$

$336.16 \times a - w(N)/w(C) \times 432.39 \times a = w(N)/w(C) \times 288.26$

$a = w(N)/w(C) \times 288.26 : (336.16 - w(N)/w(C) \times 432.39)$

$w(N)/w(C) = 0.2590$

giving a = 0. 333

Then with **a = 0. 333** the total molecular weight of the composite $[Cr_3OCl(H_2O)_2(C_8H_4O_4)_3][C_{36}H_{36}N_{24}O_{12}]_{0.333}$ is 1067.77 g/mol.

For this, the calculated weight-% of H is 2.65; to be compared with found H 2.82%.

Thus, the weight percentage of CB6 in the CB6@MIL-101-Cl then is $(0.333 \times 996.84 / 1067.77) \times 100\% = 31$ wt%.

The composition of the composite was assessed in previous work based on elemental analysis data and digestion NMR as 29 wt% of CB6 in MIL-101(Cr).[1]

Scheme S1 Setup for humid SO_2 exposure experiments. a) SO_2 sensor, b) Hygrometer, c) Flowmeter, d) Natrium metabisulfite solution ($Na_2S_2O_5$), e) Sodium chloride solution, f) H_2O.

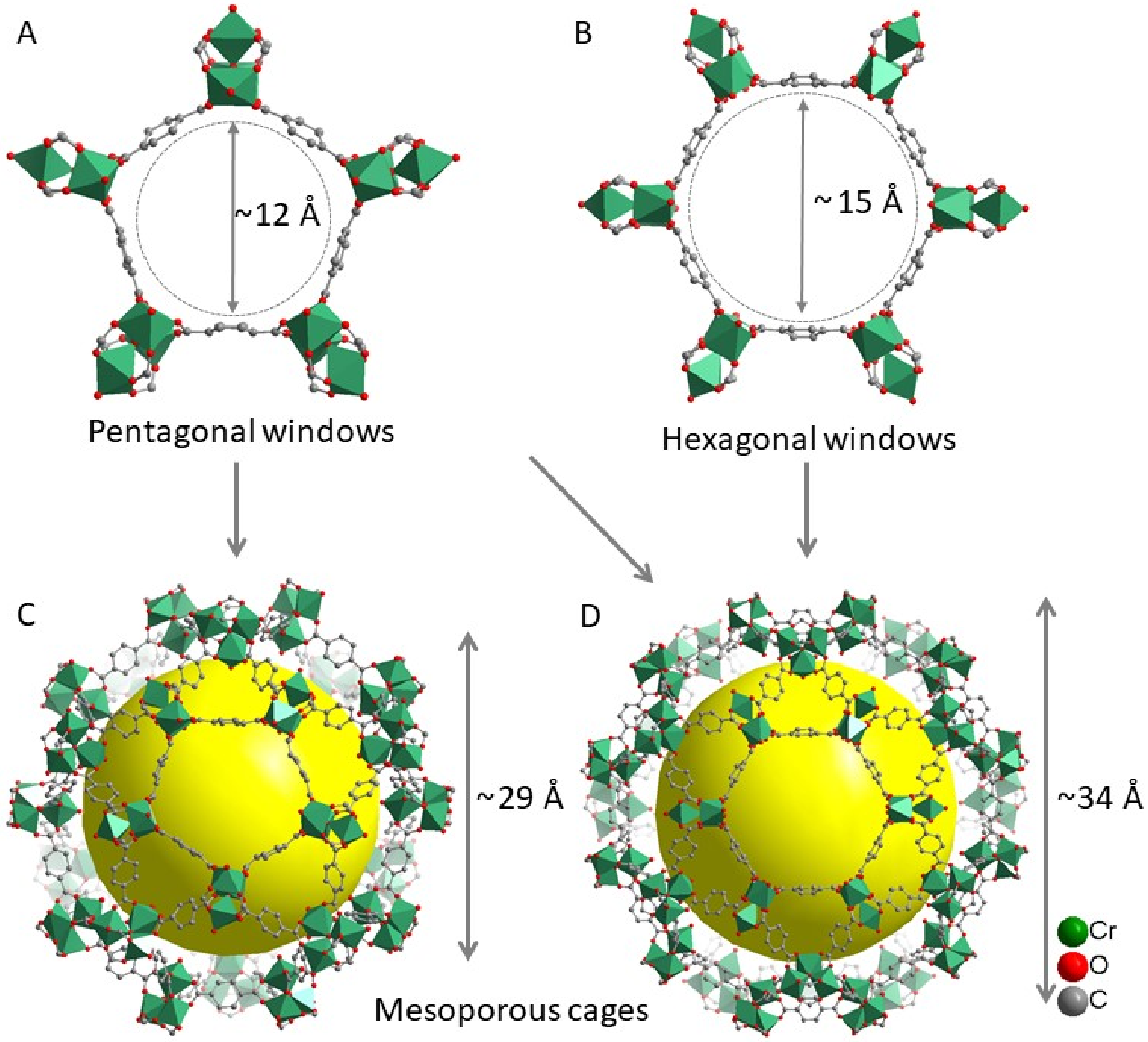

Scheme S2 Schematic representation of the MIL-101 structure. Graphics have been drawn with the software DIAMOND from the deposited cif-files under CCDC no. 605510, Refcode OCUNAC for MIL-101(Cr).[2]

Table S2 Textural properties of MIL-101, CB6@MIL-101-Cl and nanoCB6-H.

	S_{BET} [a] [$m^2 \cdot g^{-1}$]	V_{total} [b] [$cm^3 \cdot g^{-1}$]	V_{micro} [c] [$cm^3 \cdot g^{-1}$]
MIL-101	3217	1.54	1.17
CB6@MIL-101-Cl	2077	1.00	0.81
nanoCB6-H	435	0.24	0.11

[a] BET surface area was determined over 7 points in the relative pressure range p/p_0 = 0.05–0.2 from N_2 sorption isotherms at 77K for MIL-101 and CB6@MIL-101-Cl (p/p_0 =0.02–0.08 for nanoCB6-H).

b Total pore volumes (V_{total}) were determined from N_2 sorption isotherms at 77 K (p/p_0 = 0.90).

c Micropore volumes were determined using the t–plot method from five adsorption points in the pressure range p/p_0 = 0.2 - 0.4 based on N_2 adsorption curves at 77 K.

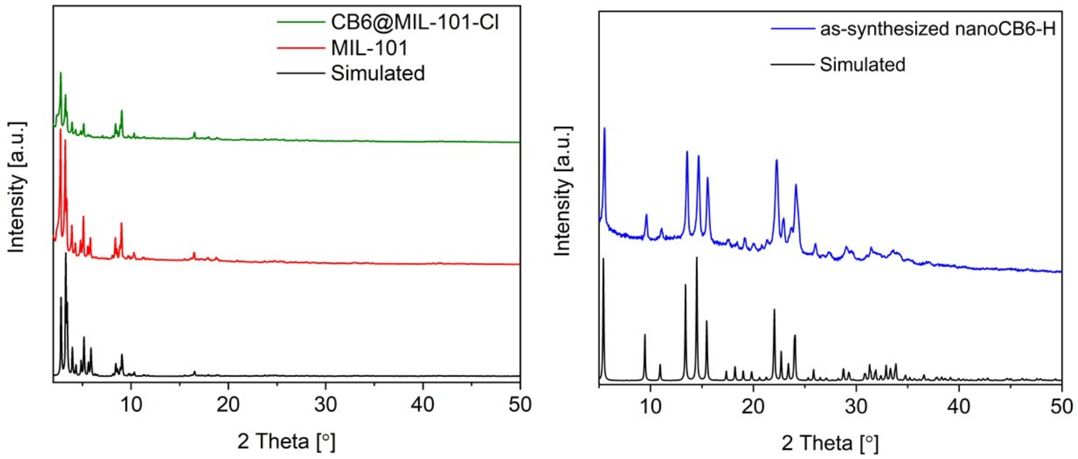

Fig. S1 PXRD patterns of MIL-101, composite CB6@MIL-101-Cl (left) and nanoCB6-H (right). Simulations from the deposite cif file with CCDC no. 605510, Refcode OCUNAC for MIL-101(Cr)[2] and with CCDC no. 676880, Refcode KOBNEV for CB6-H.[3]

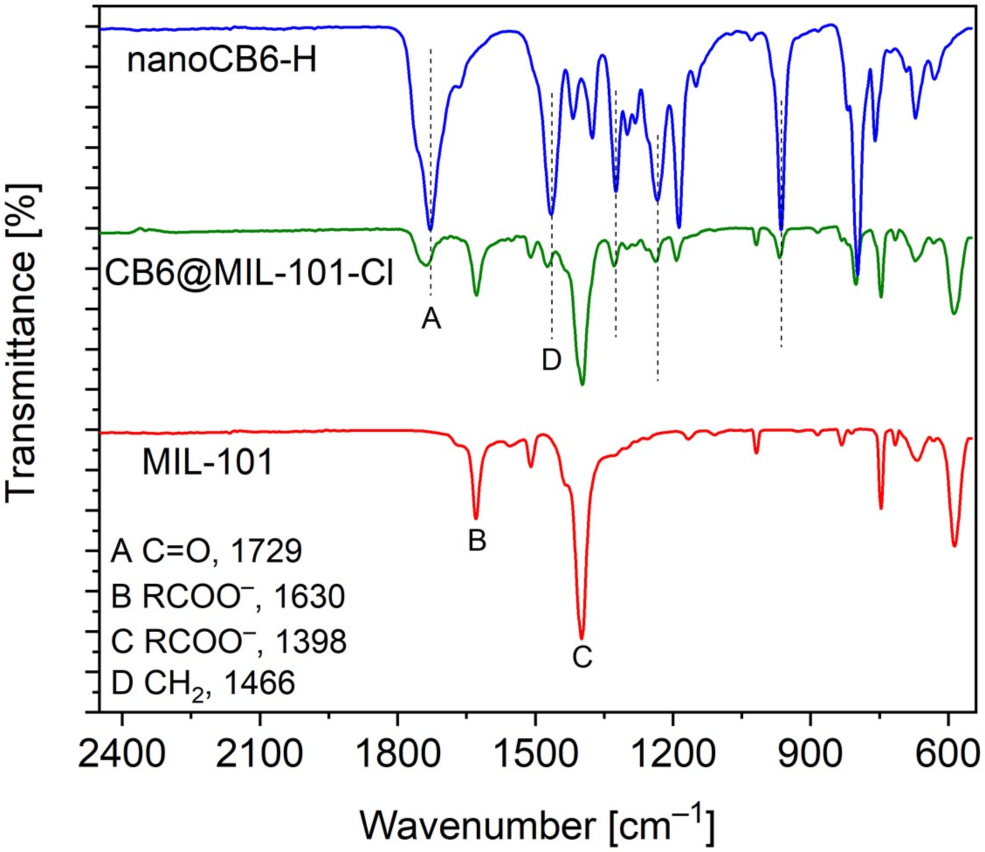

Fig. S2 FT-IR spectra of nanoCB6-H, MIL-101 and CB6@MIL-101-Cl.

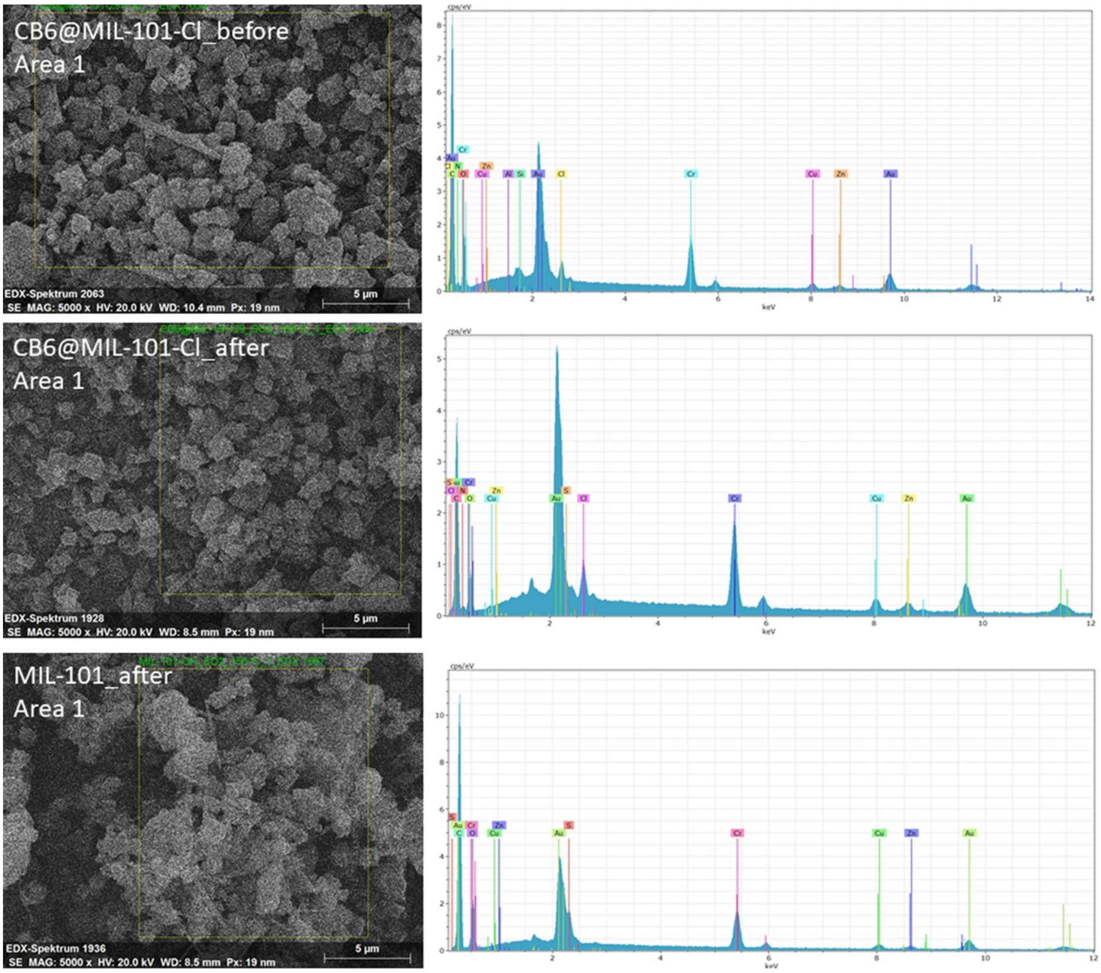

Fig. S3 SEM images and corresponding EDX spectra of CB6@MIL-101-Cl and MIL-101 before and after one-cycle of SO_2 adsorption-desorption. Area 1 (whole region) is shown here as the example for other two areas (part region).

In CB6@MIL-101-Cl, EDX cannot be used for sulfur quantification due to the vicinity/ overlap of the Au and S peak. It is evident that the samples before SO_2 sorption also exhibit the same "S shoulder" due to the strong background signal in this energy region.

Table S3 EDX-based elemental composition of Cl/Cr_3 atom-group ratios in CB6@MIL-101-Cl and MIL-101 before and after one-cycle of SO_2 adsorption-desorption.[a]

			Cr [At%]	**Cl [At%]**	**Cl/Cr**	**Cl/Cr_3 (Aver.)**
CB6@MIL-101-Cl	before	Area 1	2.46	0.55	0.22	0.78
		Area 2	3.22	0.93	0.29	
		Area 3	2.71	0.74	0.27	
	after	Area 1	4.78	1.15	0.24	0.69
		Area 2	2.47	0.56	0.23	
		Area 3	1.05	0.23	0.22	
MIL-101	after	Area 1	2.41	—	—	—
		Area 2	3.15	—	—	
		Area 3	3.09	—	—	

[a] The concomitant SEM images and EDX spectra are shown in Fig. S3.

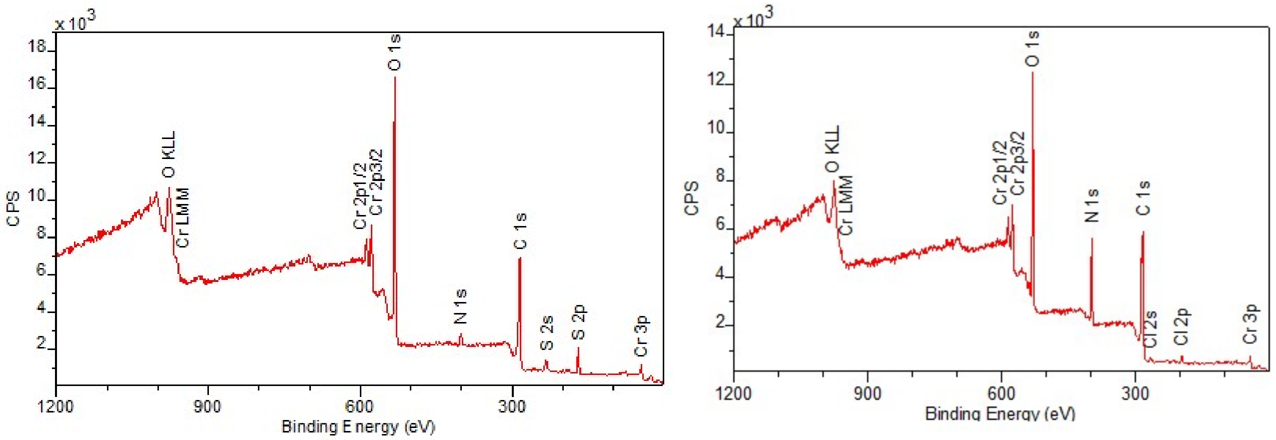

Fig. S4 XPS survey spectra of MIL-101 (left) and CB6@MIL-101-Cl (right). The trace amount of nitrogen in MIL-101 is due to the residual DMF solvent, which was used for washing the samples.

Table S4 XPS-based elemental composition of Cl/Cr$_3$ and S/Cr$_3$ atom-group ratios in CB6@MIL-101-Cl and MIL-101 after one-cycle of SO$_2$ adsorption-desorption.

	Cr		**Cl**		**S**		**Cl/Cr$_3$**	**S/Cr$_3$**
	Area	**At%**	**Area**	**At%**	**Area**	**At%**		
CB6@MIL-101-Cl	123.08	2.58	44.33	0.93	—	—	1.08	—
MIL-101	181.88	3.56	—	—	256.53	5.02	—	4.23

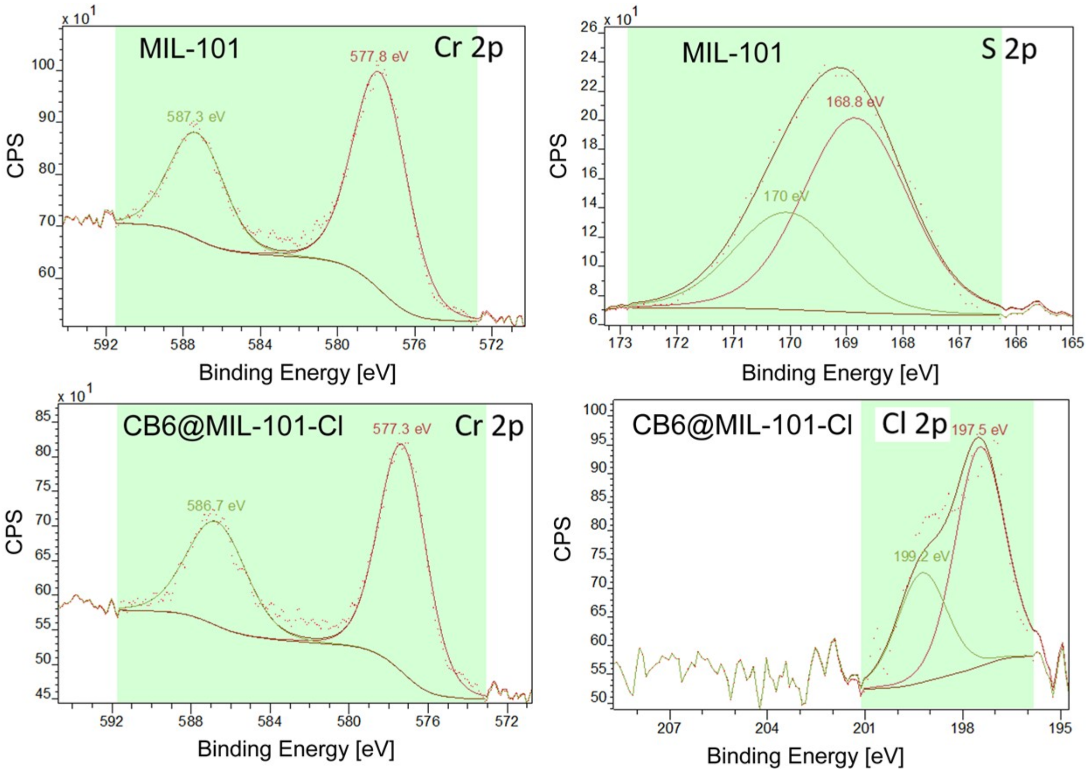

Fig. S5 High-resolution Cr 2p XPS spectra of MIL-101 and CB6@MIL-101-Cl, high-resolution S 2p spectrum in MIL-101 and high-resolution Cl 2p spectrum in CB6@MIL-101-Cl after one-cycle of SO$_2$ adsorption-desorption followed by activation at 150 °C under vacuum.

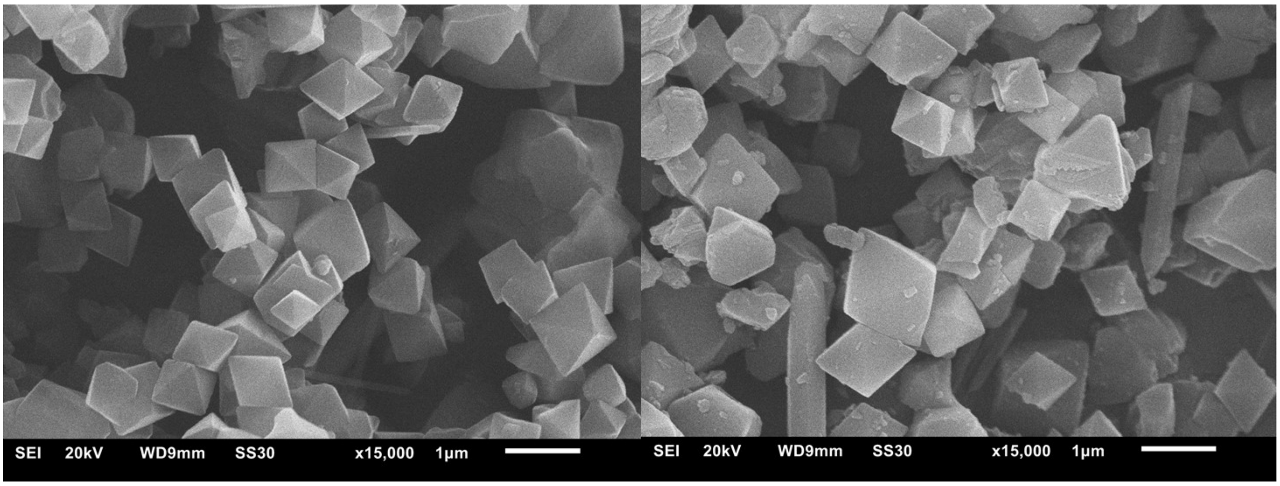

Fig. S6 Scanning electron microscopy (SEM) images for MIL-101 (left) and CB6@MIL-101-Cl (right). The scale bar in both images is 1µm.

SO_2-sorption isotherm fitting

The fitting of adsorption isotherms of SO_2 yields affinity constants. Fitting-simulations were calculated using the 3P sim software.[4] We applied the dual-site Langmuir (DSL) model (eq. S1) on the isotherm data. Fitting parameters are shown in Table S5.

DSL:
$$q_{eq} = q_{max1}\frac{\cdot K_1 \cdot p}{1 + K_1 \cdot p} + q_{max2}\frac{\cdot K_2 \cdot p}{1 + K_2 \cdot p} \qquad \text{(S1)}$$

q_{eq}= amount adsorbed [mmol g^{-1}]

q_{max} = maximum adsorption capacity [mmol g^{-1}]

K_1, K_2 = affinity constant for adsorption at site 1, 2 [1/bar]

p = pressure [kPa]

Table S5 Dual-site Langmuir fitting parameters for SO_2 at 293 K calculated using 3P sim software.[a,4]

	Model	R^2	Affinity const. K_1 [1/bar]	Max. loading 1 [mmol g^{-1}]	Affinity const. K_2 [1/bar]	Max. loading 2 [mmol g^{-1}]
CB6@MIL-101-Cl	DSL	0.999	78.282	4.323	0.378	57.502
MIL-101	DSL	0.999	3.083	12.335	0.302	82.750
nanoCB6-H	DSL	0.998	427.341	3.488	0.522	8.694

[a] DSL_ Dual-site Langmuir. The number of three decimal digits may be needed for the IAST selectivity calculation. Rounding to one decimal digit leads to significant deviations in the IAST values. The corresponding fitting curves are shown in Fig. S7.

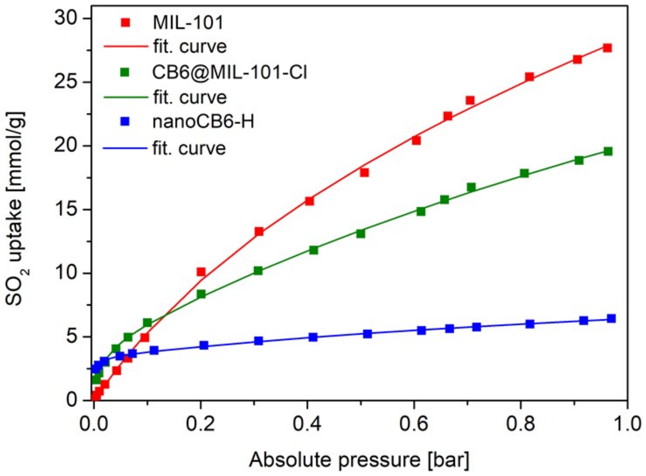

Fig. S7 Experimental SO_2 sorption isotherm at 293 K and corresponding fitting curves of MIL-101 (red), CB6@MIL-101 (green) and nanoCB6-H (blue).

Table S6 Comparison of SO_2 sorption data for MOFs.

The criteria for the stability and/or durability of MOFs are based on the combination of the unchanged PXRD pattern and a decrease in surface area by less than 10% after dry and humid SO_2 compared to the pristine MOF. In addition or alternatively, the maximal SO_2 uptake of multiple individual gas adsorption measurements or the cyclic breakthrough measurement decreased by less than 20% at the second run and kept an insignificant uptake change in the following runs.

Material	BET surface area [$m^2 \cdot g^{-1}$]	SO_2 uptake [$mmol \cdot g^{-1}$]		Temp. [K]	Stability and/or reusability	Reference
		0.01 bar	1 bar			
CB6@MIL-101-Cl	2077	2.2	19.5	293	yes	This work
		2.0	17.0	298		This work
nanoCB6-H	435	2.8	6.5	293	no	This work
MIL-101	3217	0.7	27.7	293	no	This work
		0.6	24.4	298		This work
SIFSIX-2-Cu-i	630	4.2	6.9	298	yes [c]	5
MIL-160	1170	4.2	7.2	293	yes [d]	6
DMOF-TM	900	3.8	9.7	293	yes [e]	7
SIFSIX-1-Cu	1337	3.4	11.01	298	yes [f]	5
MFM-305	779	3.3[a]	7	298	unclear [g]	8
$MFM\text{-}305\text{-}CH_3$	256	3[a]	5.2	298	unclear [g]	8
NH_2-MIL-125(Ti)	1560	3	10.8	293	no [h]	6
mmen-MIL-101(Cr)	2377	3	—	298	yes [i]	9
SIFSIX-3-Ni	223	2.4	2.7	298	probably no [j]	5
MOF-808	1190	2.1	14.6	293	no [k]	10
NH_2-MIL-53(Al)	1120	2.0	8.0	293	no [l]	10
HKUST-1	1490	2.0	13.8	293	yes	11
SIFSIX-3-Zn	250	1.7	2.1	298	probably no [j]	5

Material	BET surface area [m^2·g^{-1}]	SO_2 uptake [mmol·g^{-1}]		Temp. [K]	Stability and/or reusability	Reference
		0.01 bar	1 bar			
MFM-300(In)	1071	1.6[a]	8.28	298	yes [m]	12
MFM-601	3644	1.6[a]	12.3	298	/	13
NH_2-MIL-101(Al)	1770	1.5	17.3	293	no[n]	10
Mg-MOF-74	1206	1.4[a]	8.6	298	/	14,15
Zr-Fum	600	1.3	6.5	293	yes	10
MIL-101(Cr)-4F(1%)	2176	1.3[a]	18.4	298	yes	16
NH_2-MIL-101(Cr)	2290	1.2	16.7	293	no	11
CAU-10-H	600	1.2	4.8	293	no	10
MIL-96(Al)	530	1.2	6.5	293	no[n]	10
Al-Fum	970	1.0	7.5	293	no	10
[Zn_2(L1)$_2$(bpe)]	275	0.7[a]	6.4	293	yes (only PXRD)	17
Basolite F300	1070	0.6	9.5	293	no	11
MFM-170	2408	0.5[a]	17.5	298	yes	18
MFM-202a	2220	0.4[a]	10.2[b]	298	no	19
Ni(bdc)(ted)$_{0.5}$	1738	0.3[a]	10	298	yes (only PXRD)	15
MOF-177	4100	0.25	25.7	293	no	6

[a] Estimated from isotherm [b] MFM-202a undergoes a distinct irreversible framework phase transition upon SO_2 uptake at 268−283 K to give MFM-202b which has enhanced stability.

[c] The breakthrough performance did not decline through cyclic breakthrough tests for 6 cycles, PXRD indicates the stability after breakthrough.

[d] Evaluated by multiple individual SO_2 sorption runs. MIL-160 shows stability with insignificant reduction of the gas uptake over 5 runs.

[e] The sample was exposed to dry and humid SO_2 for 6 hours, respectively. Its stability was evaluated from PXRD and BET surface area (90%), and from the breakthrough experiments for 3 cycles.

[f] The breakthrough performance did not decline through cyclic breakthrough tests for 4 cycles, PXRD indicates the stability after breakthrough.

[g] For MFM-305 and MFM-305-CH_3, no experimental data or graphic for stability is found, only one sentence refers to the stability: “the SO_2 uptake is fully reversible in both materials, and no loss of crystallinity or porosity was observed for the regenerated samples.”

[h] NH_2-MIL-125(Ti) displayed a reduced SO_2 uptake in the second run and then stabilized its adsorption capacity at the third run. The surface area of NH_2-MIL-125 deceased by about 20% under dry and humid SO_2. In the second SO_2 run, the maximal SO_2 uptake decreased by 22%.

[i] The sample after exposure to pure SO_2 was evaluated by PXRD and N_2 adsorption, which indicated the crystalline and porosity of the sample were preserved. Cyclic breakthrough experiment displayed a SO_2 uptake in the second run (83%) and then kept unchanged during 5 cycles.

[j] In the combined work is mentioned that “SIFSIX-1-Cu and SIFSIX-2-Cu-i fulfill the requirements by FGD technology, natural-gas purification and other SO_2-separation processes for both SO_2 capacity and selectivity.” but there is no experimental stability data of SIXSIF-3-Ni and SIFSIX-3-Zn given.

[k] Under dry SO_2 exposure, MOF-808 is stable, but after humid SO_2 exposure, the surface area decreased to about 65%.

[l] After humid SO_2 exposure, the surface area of NH_2-MIL-53(Al) decreased by more than 50%.

[m] MFM-300(In) displays complete retention of the framework structure upon contact with SO_2, H_2SO_3, and H_2SO_4 (verified by PXRD and SEM), demonstrating the excellent stability of this material for SO_2 capture in both dry and humid conditions.

[n] Under dry SO_2 exposure, NH_2-MIL-100(Al) and MIL-96(Al) had already demonstrated a major loss of porosity, and thus were deemed SO_2-unstable.

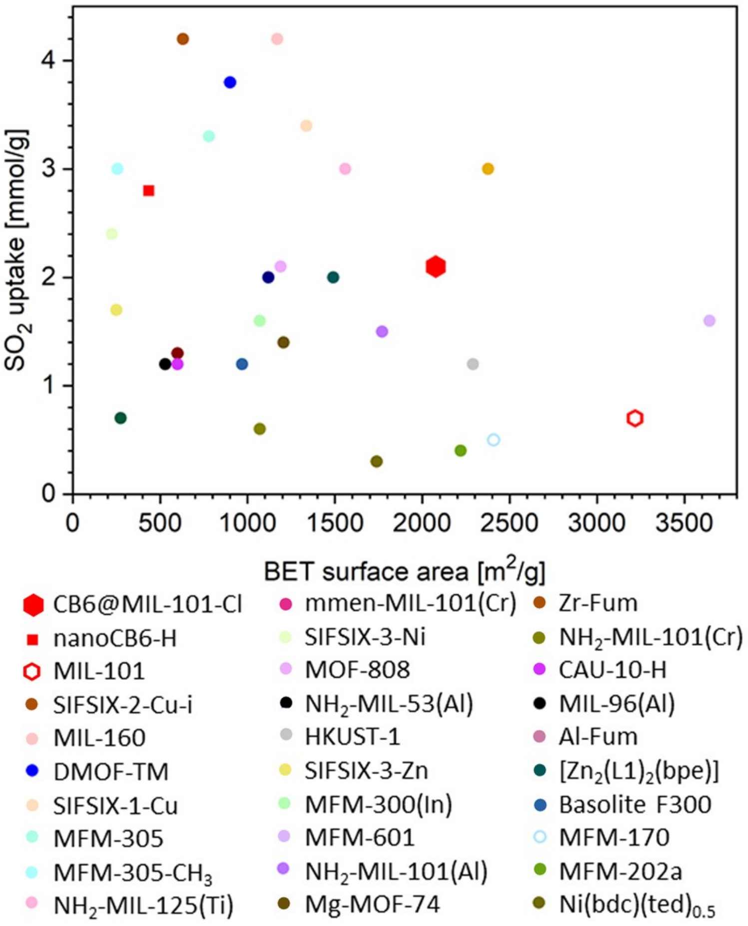

Fig. S8 Comparison of SO$_2$ uptakes of reported MOFs at 0.01 bar and 293 K or 298 K. Plot of SO$_2$ adsorption against BET surface area (Open symbols denote the possible presence of open metal sites in the MOF).

Isosteric enthalpy of adsorption

Virial analysis

To calculate the isosteric enthalpy of adsorption (ΔH_{ads}) for SO_2 isotherm data, we applied the virial method to fit the adsorption data simultaneously at 273 K and 293 K in Origin from equation (eq. S2)[20] (Ref. OriginLab Corporation, OriginPro, Version 9.0.0G., OriginLab Corporation 1991-2012.).

$$ln(P) = ln(n) + \frac{1}{T}\sum_{i=0}^{m} a_i n^i + \sum_{i=0}^{m} b_i n^i \qquad \text{(S2)}$$

In Eq. (1), *P* is the pressure in kPa, *n* is the total amount adsorbed in mmol/g, *T* is the temperature in K (here 273K, 293K), a_i and b_i are virial coefficients, and *m* stands for the number of coefficients required to adequately fit the isotherms.

Therefore, ΔH_{ads} can be calculated from equation (eq. S3), where *R* is the universal gas constant.

$$\Delta H_{ads} = - Q_{st} = R\sum_{i=0}^{m} a_i n^i \qquad \text{(S3)}$$

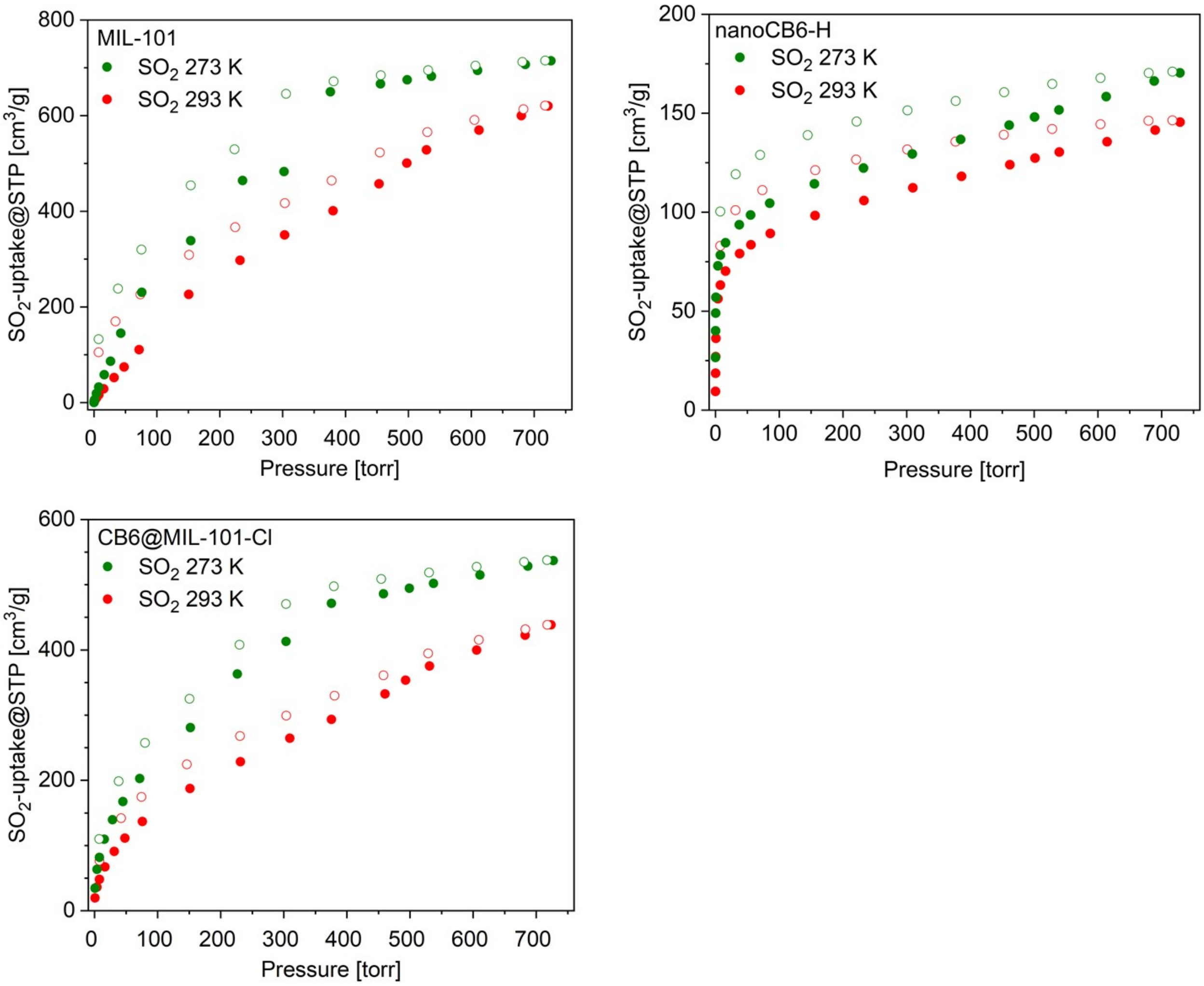

Fig. S9 SO_2 adsorption isotherms of MIL-101, nanoCB6-H and CB6@MIL-101-Cl at 293 K and 273 K.

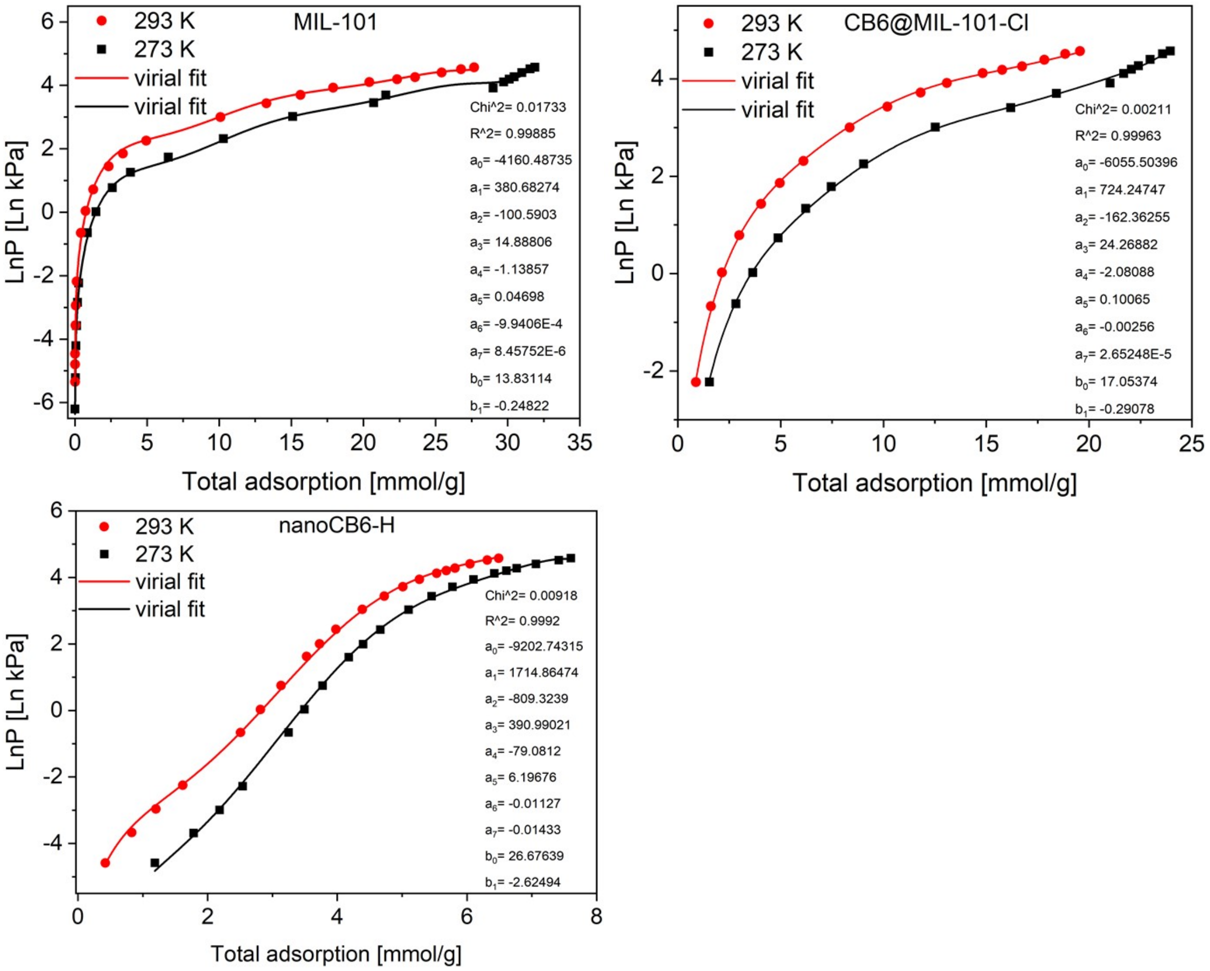

Fig. S10 Virial analysis for heat of adsorption of MIL-101, CB6@MIL-101-Cl and nanoCB6-H from SO_2 adsorption at 273 K and 293 K.

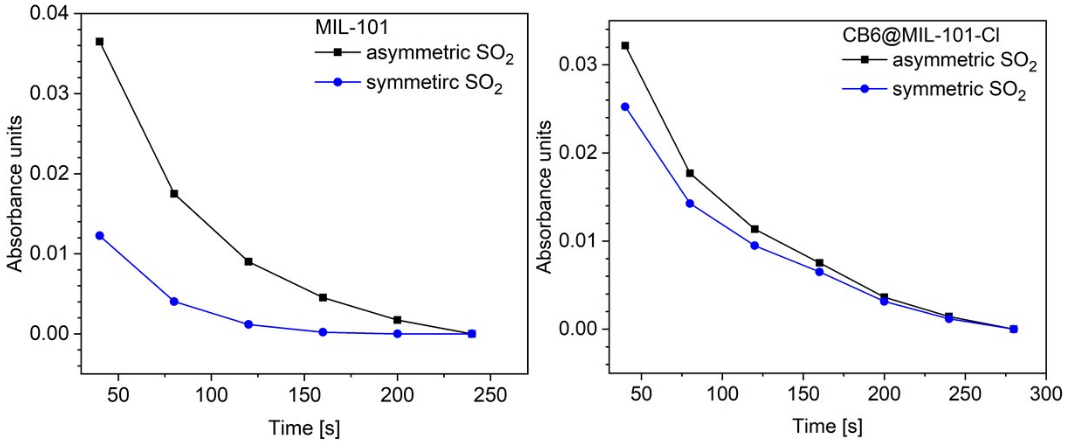

Fig. S11 Intensity change of absorbance bands at ~1330 (black) and ~1144 cm^{-1} (blue) of MIL-101 (left) and CB6@MIL-101-Cl (right) as a function of time, corresponding to the asymmetric and symmetric stretching vibration of physisorbed SO$_2$.

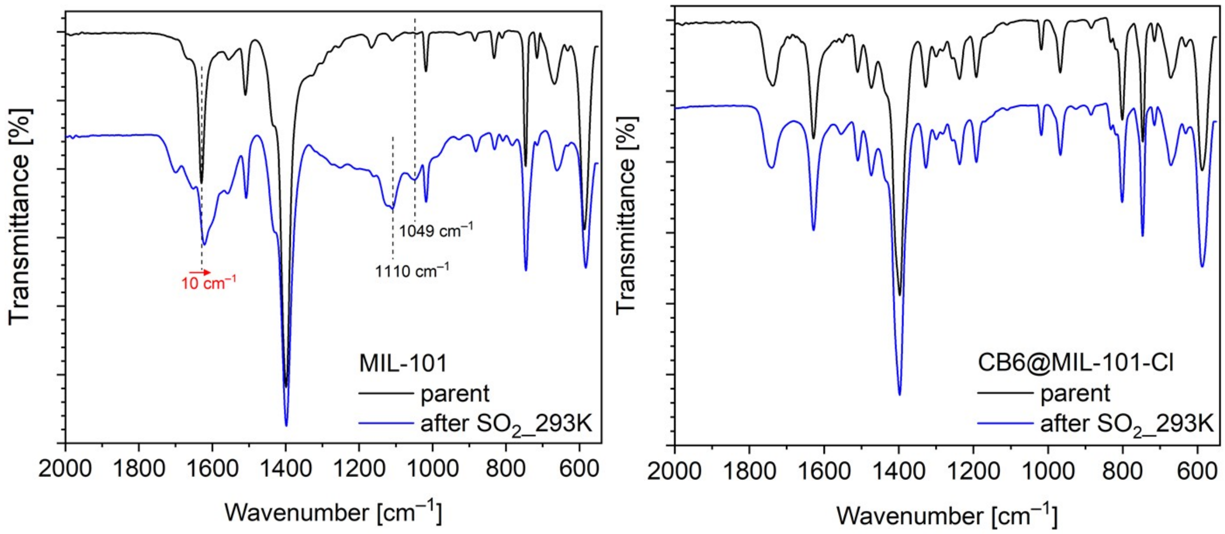

Fig. S12 FT-IR spectra of MIL-101 and CB6@MIL-101-Cl before and after one-cycle full SO$_2$ adsorption-desorption at 293 K followed by degassing at 150 °C and 1×10^{-3} mbar for 12 h. We note that the peak at slightly below 700 cm^{-1} in MIL-101 and CB6@MIL-101 exists in non-degassed samples prior to FT-IR measurements, however, it vanishes when the sample is well degassed directly prior to the measurement.

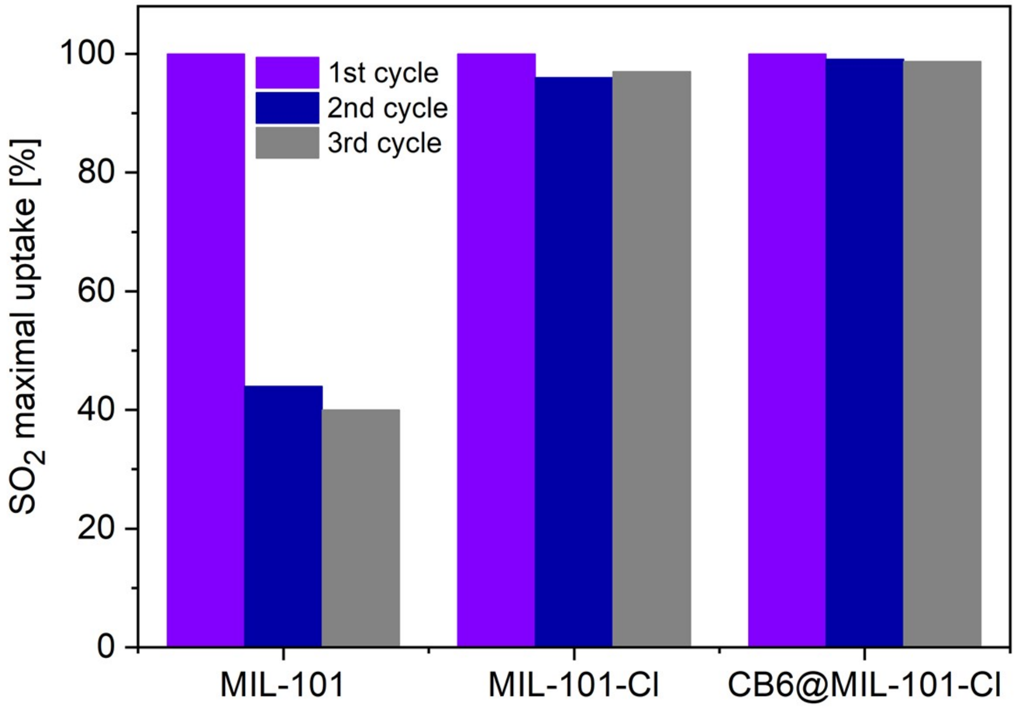

Fig. S13 Cycling SO$_2$ adsorption-desorption performance of MIL-101[21], MIL-101-Cl and CB6@MIL-101-Cl at 293 K and 0.96 bar from three-cycle ad/desorption measurements, full isotherms (with 17 points for ads. and 12 points for des.). Between each individual isotherm sorption experiment the samples were activated at 150 °C under vacuum (1×10^{-3} mbar) for 12 hours. The first SO$_2$ uptake value was set to 100% as reference point with the second and third uptake value given relative to it.

Table S7 Porosity characteristics of MIL-101, CB6@MIL-101-Cl, MIL-101-Cl and nanoCB6-H before and after exposure to cyclic SO$_2$ adsorption at 293 K, and after exposure to humid SO$_2$ for 6 h.

	before		**after cyclic SO$_2$ ads.**		**after humid SO$_2$ exposure**	
	S_{BET} [$m^2 \cdot g^{-1}$]	V_{total} [$cm^3 \cdot g^{-1}$]	S_{BET} [$m^2 \cdot g^{-1}$]	V_{total} [$cm^3 \cdot g^{-1}$]	S_{BET} [$m^2 \cdot g^{-1}$]	V_{total} [$cm^3 \cdot g^{-1}$]
MIL-101	3217	1.54	1768	0.84	3228	1.50
CB6@MIL-101-Cl	2077	1.00	2036	0.98	2104	1.03
MIL-101-Cl	3408	1.63	3541	1.66	3390	1.63
nanoCB6-H	435	0.24	—	—	79	0.06

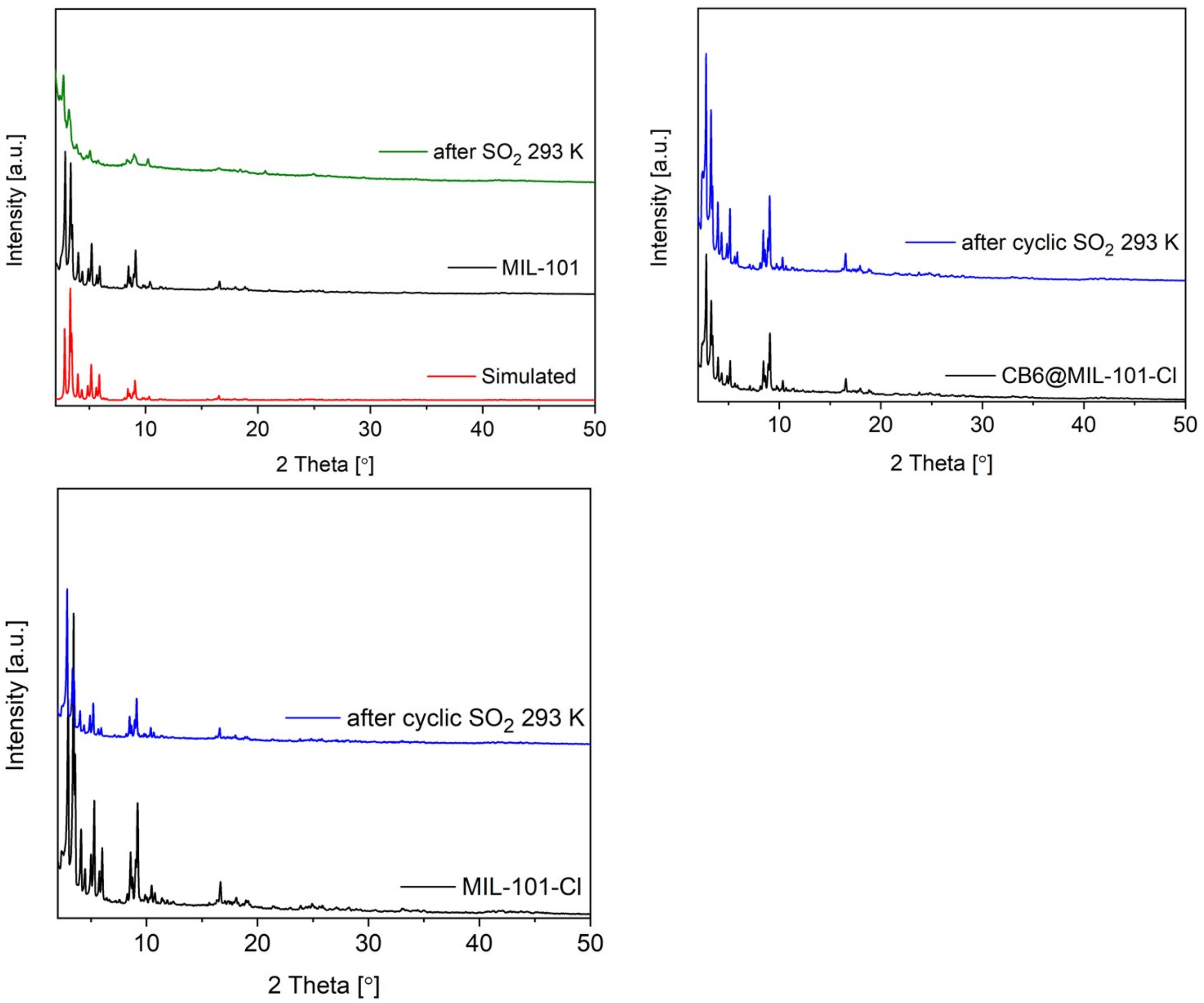

Fig. S14 PXRD patterns of MIL-101, CB6@MIL-101-Cl and MIL-101-Cl after cyclic SO_2 adsorption (3 cycles for MIL-101 and MIL-101-Cl, 10 cycles for CB6@MIL-101-Cl. The samples between each individual sorption experiment were activated at 150 °C and $1{\times}10^{-3}$ mbar. After the last cycle each sample was degassed at 150 °C and 1×10^{-3} mbar for 12 h.

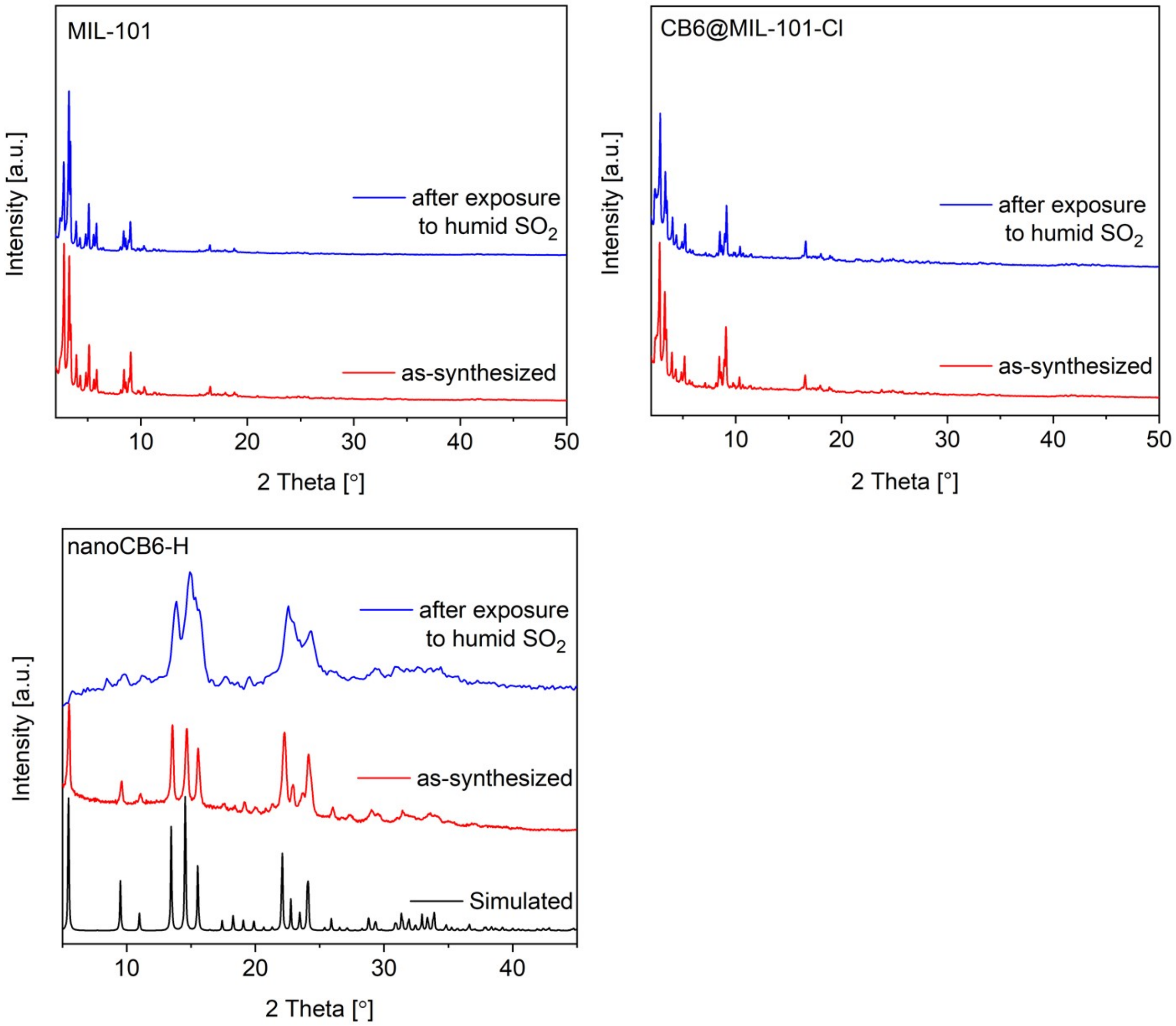

Fig. S15 PXRD patterns of MIL-101, CB6@MIL-101-Cl and nanoCB6-H before and after exposure to humid SO_2 (35 ± 5 ppm) for 6h.

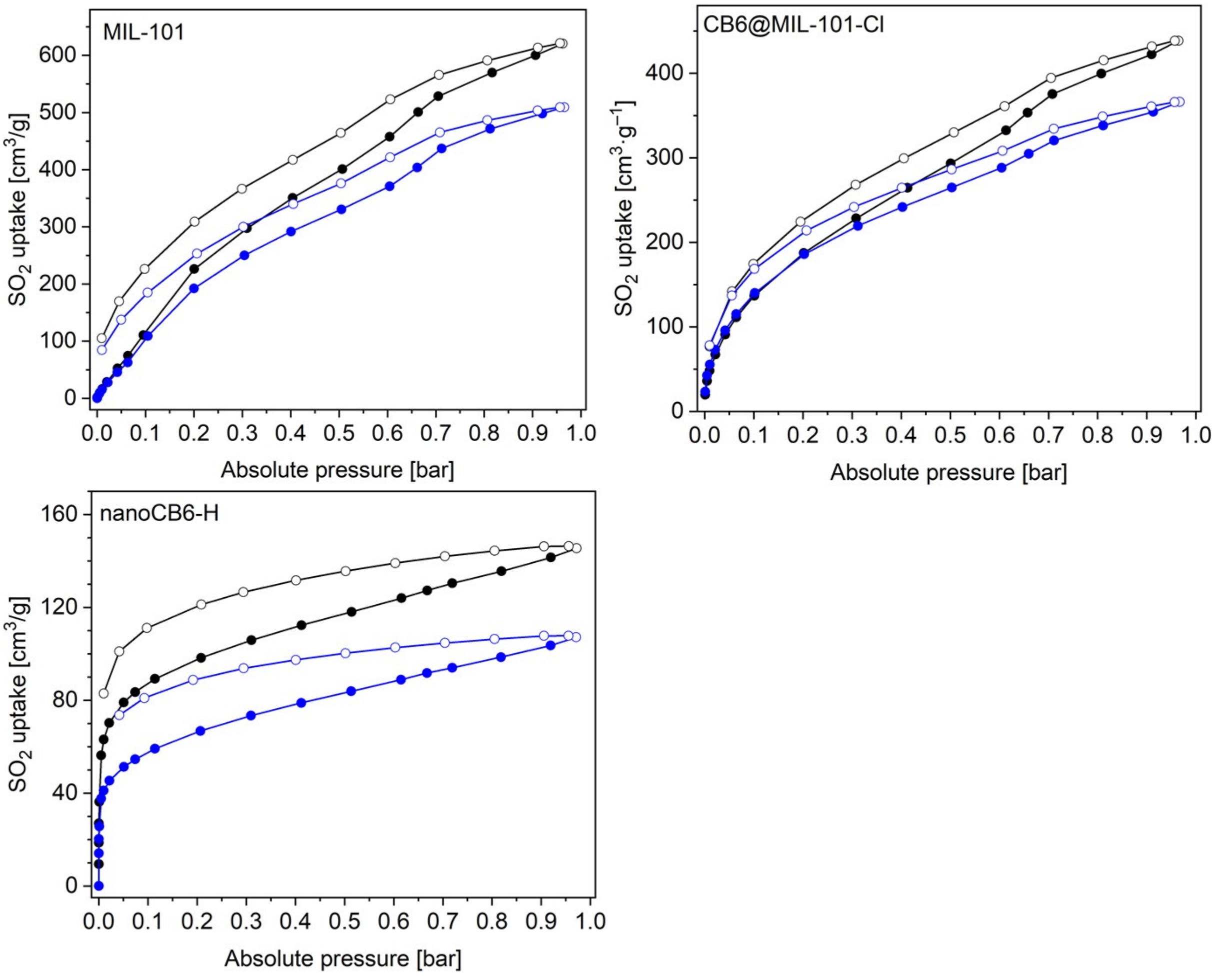

Fig. S16 SO_2 adsorption isotherms at 293 K of MIL-101, CB6@MIL-101-Cl and nanoCB6-H before (black) and after (blue) exposure to humid SO_2 for 6 h.

Table S8 SO_2 uptake at 293K of MIL-101, CB6@MIL-101-Cl and nanoCB6-H at 0.01 bar and 1 bar.

	dry conditions		**after exposure to humid SO_2**	
	SO_2 uptake at 293 K at [$mmol \cdot g^{-1}$]		SO_2 uptake at 293 K at [$mmol \cdot g^{-1}$]	
	0.01 bar	1 bar	0.01 bar	1 bar
MIL-101	0.7	27.7	0.7	22.7
CB6@MIL-101-Cl	2.1	19.5	2.4	16.3
nanoCB6-H	2.8	6.5	1.8	4.8

References

---

[1] J. Liang, A. Nuhnen, S. Millan, H. Breitzke, V. Gvilava, G. Buntkowsky and C. Janiak, *Angew. Chem. Int. Ed.*, 2020, **59**, 6068-6073.

[2] G. Férey, C. Mellot-Draznieks, C. Serre, F. Millange, J. Dutour, S. Surblé and I. Margiolaki, *Science*, 2005, **309**, 2040.

[3] S. Lim, H. Kim, N. Selvapalam, K.-J. Kim, S. J. Cho, G. Seo and K. Kim, *Angew. Chem. Int. Ed.,* 2008, **47**, 3352-3355.

[4] 3P INSTRUMENTS, 3P sim, Version 1.1.0.7, *Simulation and Evaluation Tool for mixSorb*, 3P INSTRUMENTS 2018.

[5] X. Cui, Q. Yang, L. Yang, R. Krishna, Z. Zhang, Z. Bao, H. Wu, Q. Ren, W. Zhou, B. Chen and H. Xing, *Adv. Mater.*, 2017, **29**, 1606929.

[6] P. Brandt, A. Nuhnen, M. Lange, J. Möllmer, O. Weingart and C. Janiak, *ACS Appl. Mater. Interfaces,* 2019, **11**, 17350-17358.

[7] S. Xing, J. Liang, P. Brandt, F. Schäfer, A. Nuhnen, T. Heinen, I. Boldog, J. Möllmer, M. Lange, O. Weingart and C. Janiak, *Angew. Chem. Int. Ed.*, 2021, **60**, 17998-18005.

[8] L. Li, I. da Silva, D. I. Kolokolov, X. Han, J. Li, G. Smith, Y. Cheng, L. L. Daemen, C. G. Morris, H. G. W. Godfrey, N. M. Jacques, X. Zhang, P. Manuel, M. D. Frogley, C. A. Murray, A. J. Ramirez-Cuesta, G. Cinque, C. C. Tang, A. G. Stepanov, S. Yang and M. Schröder, *Chem. Sci.*, 2019, **10**, 1472-1482.

[9] Z. Zhang, B. Yang and H. Ma, *Sep. Purif. Technol.*, 2021, **259**, 118164.

[10] P. Brandt, S.-H. Xing, J. Liang, G. Kurt, A. Nuhnen, O. Weingart and C. Janiak, *ACS Appl. Mater. Interfaces*, 2021, **13**, 29137-29149.

[11] P. Brandt, A. Nuhnen, S. Öztürk, G. Kurt, J. Liang and C. Janiak, *Adv. Sustain. Syst.*, 2021, **5**, 2000285.

[12] M. Savage, Y. Cheng, T. L. Easun, J. E. Eyley, S. P. Argent, M. R. Warren, W. Lewis, C. Murray, C. C. Tang, M. D. Frogley, G. Cinque, J. Sun, S. Rudić, R. T. Murden, M. J. Benham, A. N. Fitch, A. J. Blake, A. J. Ramirez-Cuesta, S. Yang and M. Schröder, *Adv. Mater.*, 2016, **28**, 8705-8711.

[13] J. H. Carter, X. Han, F. Y. Moreau, I. da Silva, A. Nevin, H. G. W. Godfrey, C. C. Tang, S. Yang and M. Schröder, *J. Am. Chem. Soc.*, 2018, **140**, 15564-15567.

[14] T. Grant Glover, G. W. Peterson, B. J. Schindler, D. Britt and O. Yaghi, *Chem. Eng. Sci.*, 2011, **66**, 163-170.

[15] K. Tan, P. Canepa, Q. Gong, J. Liu, D. H. Johnson, A. Dyevoich, P. K. Thallapally, T. Thonhauser, J. Li and Y. J. Chabal, *Chem. Mater.*, 2013, **25**, 4653-4662.

[16] E. Martínez-Ahumada, M. L. Díaz-Ramírez, H. A. Lara-García, D. R. Williams, V. Martis, V. Jancik, E. Lima and I. A. Ibarra, *J. Mater. Chem. A*, 2020, **8**, 11515-11520.

[17] S. Glomb, D. Woschko, G. Makhloufi and C. Janiak, *ACS Appl. Mater. Interfaces,* 2017, **9**, 37419-37434.

[18] G. L. Smith, J. E. Eyley, X. Han, X. Zhang, J. Li, N. M. Jacques, H. G. W. Godfrey, S. P. Argent, L. J. McCormick McPherson, S. J. Teat, Y. Cheng, M. D. Frogley, G. Cinque, S. J. Day, C. C. Tang, T. L. Easun, S. Rudić, A. J. Ramirez-Cuesta, S. Yang and M. Schröder, *Nat. Mater.,* 2019, **18**, 1358-1365.

[19] S. Yang, L. Liu, J. Sun, K. M. Thomas, A. J. Davies, M. W. George, A. J. Blake, A. H. Hill, A. N. Fitch, C. C. Tang and M. Schröder, *J. Am. Chem. Soc.*, 2013, **135**, 4954-4957.

[20] A. Nuhnen and C. Janiak, *Dalton Trans.,* 2020, **49**, 10295-10307.

[21] N. Tannert, Y. Sun, E. Hastürk, S. Nießing and C. Janiak, *Z. Anorg. Allg. Chem.*, 2021, **647**, 1124–1130.